Size and Shape Optimization of Structured-Wall PE Pipes in Ringstiffness Tests

F. Fuerle, J. Sienz and M. Innocente
Civil and Computational Engineering Centre, School of Engineering, Swansea University, Singleton Park, Swansea, SA2 8PP, UK

V. Samaras and S. Thomas
Asset International Ltd., Stephenson Street, Newport, NP19 4XH, UK.

Structured-wall high density polyethylene pipes up to 3m diameter are used extensively in civil engineering applications including storm water attenuation tanks, culverts, surface drainage, inter-process pipe work, sewers. A key quality control measure for the manufacture of such pipes is the ringstiffness to BS EN 1446: 1996. The ability to predict this accurately and inexpensively as a function of the pipe wall geometry is a pre-requisite for optimization of the pipe design. The paper describes the development of Finite Element modeling of the ringstiffness test as well as an optimization procedure containing open-source and in-house software only. The material saving capabilities will be discussed by means of two optimization examples.

Nomenclature

A	=	area that springs are attached to
b_i	=	*i*-th control value for B-spline
B_i	=	*i*-th control point for B-spline
D	=	internal diameter of pipe
DV_i	=	*i*-th design variable
f	=	objective function or constraint
F	=	force in ringstiffness test
h	=	height of cross-section
L	=	length of pipe sample
n_{DV}	=	number of design variables
n_{Spring}	=	number of springs
lps	=	lateral pipe stiffness
SN	=	ringstiffness
S_{Spring}	=	spring stiffness
R_i	=	inner radius of the pipe
R_o	=	outer radius of the pipe
y	=	pipe deflection
ξ	=	perturbation factor

I. Introduction

The structured wall pipes studied within the present work are produced by winding an extruded high density polyethylene (HDPE) box profile around a mandrel and welding each turn to the adjacent one (see Fig. 1). The main objectives of the current study are the development of a fast and accurate numerical simulation of the standardized ring flexibility test according to the standard BS EN 1446: 1996 and, using this simulation, the

development of an optimization procedure capable of size and shape optimization as well as its application. For more information regarding the standard the reader is referred to Ref. 1. This standard specifies a method to measure the flexibility of a thermoplastic pipe with a circular cross section. To conduct such a test, an approximately 1-meter-wide pipe sample is placed in a compression testing machine, as shown in Fig. 2.

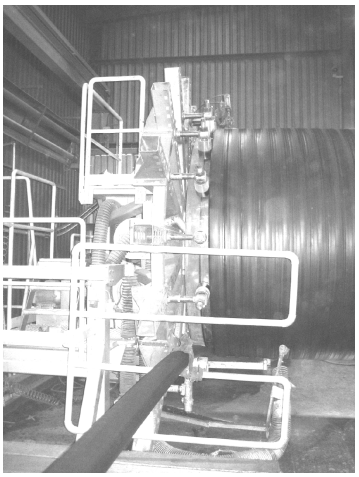

Figure 1: The profile is wound around a mandrel and welded to the adjacent one.

Figure 2: A pipe sample placed in the pipe stiffness machine.

When compressing the sample between the two parallel plates, the machine monitors the force (F) that is necessary to move one of the plates with constant velocity. According to the standard, the ring flexibility (SN) is calculated at a vertical deflection equal to 3% of the pipe's inner diameter, as shown in Eq. 1, where y is the vertical deflection, L is the length of the pipe sample, and D is the inner diameter.

$$SN = \frac{F \cdot \left(0.0186 + 0.025 \cdot \frac{y}{D} \right)}{y \cdot L} \tag{1}$$

Future work will look at the improvement of the pipe's performance while installation and in use. At the present stage the pipe's performance testing is restricted to that in the stiffness test.

The present paper is structured as follows: First the developed automated procedure for the generation of finite element (FE) models from scanned pipe profiles is discussed. Subsequently, several approaches to FE simulations are presented by looking at different element types and various possible boundary conditions. Furthermore, the development of an optimization procedure, consisting of open-source and in-house software only, is outlined as well as its application to a size and a shape optimization example. Finally the results of the work are presented.

II. Finite Element models and optimization procedure

A. Automated Finite Element model generation

The theoretical, rectangular box-section profiles of the pipes, extruded at the very beginning of the production process – completely defined by the height, width and wall thicknesses – significantly differ from the cross sections obtained after production, exhibiting differences of up to 20%. Therefore, it was decided to cut samples of real profiles and scan their precise cross sections.

The scanning process returns files of discrete data points, distributed over the entire cross section. These points have to be processed prior to the creation of the FE model. The programs carrying out that task are written in FORTRAN 77 and the whole procedure is controlled by means of a Java tool. The latter serves as a Graphical User Interface (GUI) and simplifies the use of the command-line-type FORTRAN programs. Furthermore, it stores and

manages the entered data. Java was chosen, since it provides a convenient way for the development of graphics, whereas FORTRAN was chosen for its known computational efficiency.

The scan processing starts with the rotation of the profile in a way that all walls are either horizontal or vertical. After that the repeating pattern can be identified, which is half of one box section. The identified repeating pattern and the rotated cross section are illustrated in Fig. 3.

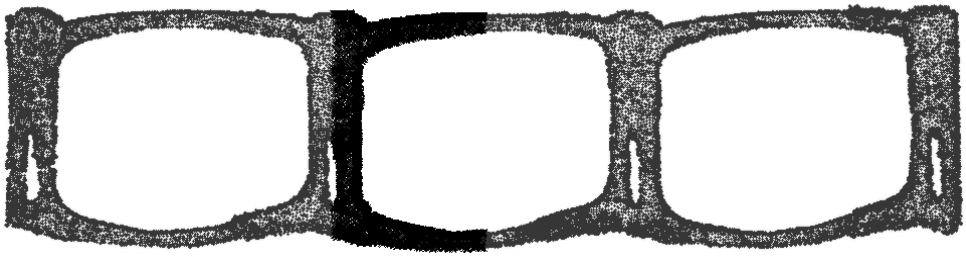

Figure 3: Rotated scanned profile with highlighted repeating pattern.

The next step is the determination of which points lie on the boundary of the cross section, since only those will be of use for the model generation. After that the boundary lines have to be smoothed so that the resulting FE model does not exhibit unreal crooked edges that can cause singularities or stress concentrations. To this end, each boundary line is replaced by a polynomial, whose parameters are found by the minimization of a least square function.

The generation of points that lie between the polynomial surface lines, and the definition of their corresponding thicknesses, are required next in order to generate an FE model with shell elements.

An FE model can now be created with solid elements using the polynomial approximation, or with shell elements using the points on the profile's midsurface line with the corresponding thicknesses. This model is then solved by the solver of choice. The procedure is summarized in Fig. 4.

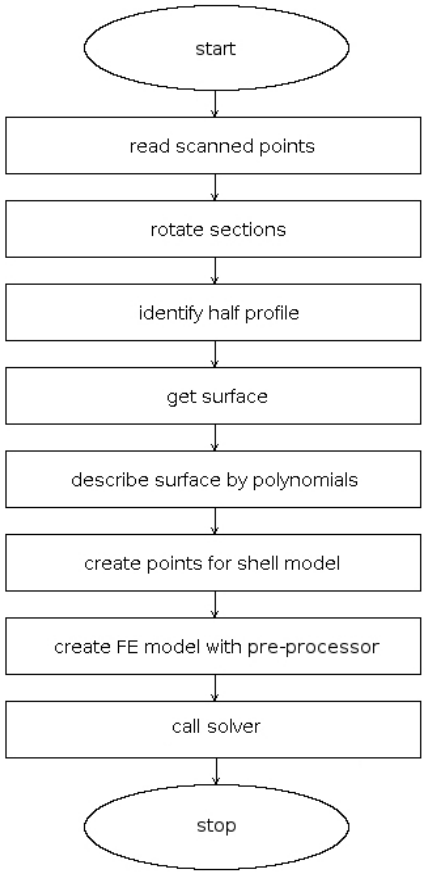

Figure 4: Flowchart of the procedure for automated FE analyses.

B. Finite Element models

This section discusses the different degrees of accuracy and efficiency that can be achieved in the simulation of the pipe stiffness test with the FE method. Numerous analyses were conducted in order to discuss and recommend a model with a suitable combination of accuracy and efficiency. For the simulations the material is modeled with an E-modulus of 1200 MPa and a Poisson's ratio of 0.4.

The two main aspects to be considered are the type of element and the correct boundary conditions. Simulations will be of the linear static type. Therefore the moving plate of the pipe stiffness experiment cannot be simulated. The constant velocity plate movement is replaced by a prescribed displacement. Furthermore, this type of simulation assumes small strain theory which is acceptable considering a pipe displacement of 3% resulting in strains of at most 0.8%.

1. Element types

Two main types of elements are considered to model this problem: "solid elements" and "shell elements". The former are 3D and describe the shape of the profile more accurately, while the latter are 2½D with a defined thickness assigned. A solid element is commonly used for 3D structures with arbitrary shapes because they can be modeled with higher precision, at the cost of a higher computational effort (refer to Fig. 5). A shell element is usually used for thin structures that present constant thicknesses. Since this is not

the case for the pipe under consideration, the cross section is divided into smaller regions with constant thicknesses assigned. Fig. 6 shows a shell model where different colors represent different thicknesses.

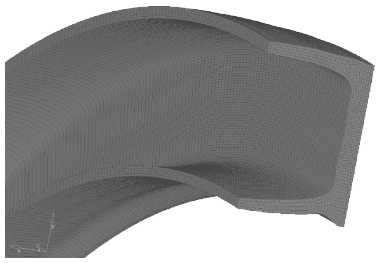

Figure 5: Solid model illustration.

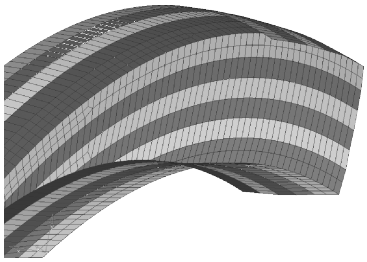

Figure 6: Shell model illustration. Different thicknesses are defined along the cross section.

On the one hand, the use of shell elements results in models with lower numbers of degrees of freedom than the use of solid elements. On the other hand, however, this introduces further simplifications to the model that might affect the accuracy of the results. While the accuracy of the global behaviour might not be jeopardized by the use of shell elements, the local behaviour certainly cannot be simulated as detailed as this is possible with solid elements. This is because the geometry cannot be represented as accurately, especially in the corners where stress concentrations are to be expected.

2. Boundary conditions

The definition of the smallest model that can accurately represent the real problem directly affects the accuracy and efficiency of the simulation. In this regard, the exploitation of symmetries and definition of appropriate boundary conditions are as challenging as critical. Clearly, both the geometry and the load state of the pipe subjected to the ringstiffness test are symmetrical with respect to all three coordinate planes. Therefore only one eighth of the whole pipe needs to be modeled, as shown in Fig. 7. The boundary conditions for this model are quite straightforward: free surface on the extreme of the pipe and no displacement on the faces cut by the symmetry planes on the directions perpendicular to them or rotations about the axes contained in such planes. Finally, the displacements of the nodes in contact with the plate must be prescribed. However, in spite of the benefits of profiting from the symmetry planes, the model is still large and computationally expensive. The geometrically repeating pattern identified in Fig. 3 makes it interesting to further reduce the model, although the geometrical symmetry is not extended to the boundary conditions. That is to say, the boundary conditions are not the same for every isolated geometrically repeating pattern. The latter, referred to as the "C profile" from here forth, is shown in Fig. 5 and Fig. 6.

Figure 7: Real repeating pattern (one eighth of the pipe).

If the C-profile is to be used to model the ringstiffness test, the question is what the appropriate boundary conditions are. A color-map of the displacements in the *x* direction for the model with the realistic symmetry exploitation (i.e. one eighth of the pipe) is shown in Fig. 8. As it can be observed, the C-profile closest to the *yz* symmetry plane (marked "A" in Fig. 8) exhibits a behaviour that resembles the one it would have if the *x*-displacements of both its faces perpendicular to the *x* axis were restricted. On the contrary, the C-profile farthest from the *yz* symmetry plane (marked "B" in Fig. 8) effectively has one face unrestricted, and the overall behaviour resembles the one it would have if its opposite face was perfectly restricted, except for the additional distortion due to the accumulated displacements.

Therefore, there is no C-profile that can realistically model the behaviour of the pipe subjected to the ringstiffness test. The best that can be aimed for is to develop some artificial boundary conditions for a C-profile – without a real counterpart – that can "represent" rather than "simulate" the real problem. That is to say, this C-profile and its boundary conditions would not be simulating any of the C-profiles in Fig. 8. It must be kept in mind that these boundary conditions are unreal.

It seems self-evident that the ringstiffness of the pipe in Fig. 7– with the real boundary conditions as described before – would be higher than that of the C-profile marked "A" in Fig. 8 having the restrictive effect of the rest of the pipe simply removed (i.e. keeping its left *yz* face unrestrained). Similarly, the ringstiffness of the whole pipe would be lower than that of the same C-profile but now having the restrictive effect of the rest of the pipe replaced by a perfect restriction (i.e. forcing the *x*-displacements of its left *yz* face to zero). Hence the C-profile with the free boundary lower-bounds the ringstiffness of the pipe in Fig. 7, while the C-profile with the restricted border upper-bounds it. However, the range of ringstiffness values bounded by these two C-models might be quite wide. Therefore, some artificial intermediate boundary condition for the left *yz* face of the C-profile "A" needs to be conceived if a C-profile is to be used to model the ringstiffness test. The great advantage of this would be that the C-model is small enough to allow numerous analyses during the optimization. The model that simulates one eighth of the pipe could be used to verify the results returned by the C-model.

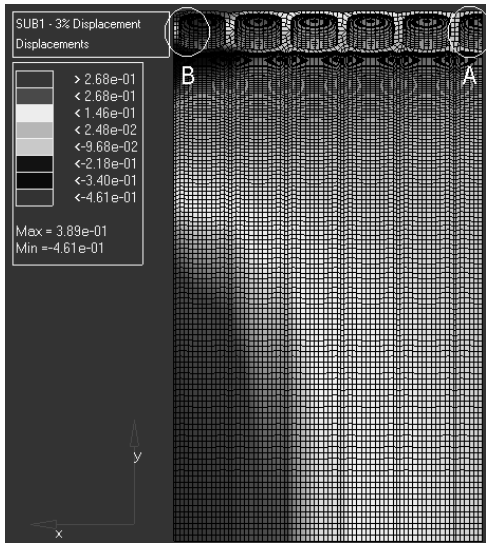

Figure 8: Component *x* of the displacements for the real repeating pattern (one eighth of the pipe).

One way to realize this desired artificial boundary condition is to use spring elements as supports at the side, where the higher or lower restrictive effect desired can be controlled by tuning the springs' stiffnesses. Thus, the latter can be adjusted in such a way that the ringstiffness obtained by using the C-profile with springs matches that of the full pipe.

It is important to keep in mind that this model cannot be used to analyze the local behaviour of specific C-profiles, but to efficiently analyze the global behaviour such as the calculation of the ringstiffness.

The spring stiffness assigned to every single spring depends upon the size of the area that every spring stands for. Thus, the concept "lateral pipe stiffness" (*lps*) is introduced in Eq. 2, where S_{Spring} is the spring stiffness, n_{Spring} is the number of springs, *A* is the area that the springs are attached to, *Ri* and *Ro* are the inner and outer radii of the pipe, and *h* is its height of the cross section.

$$lps = \frac{S_{spring} \cdot n_{spring}}{A} \tag{2}$$

$$A = h \cdot \frac{\pi}{2} \cdot \frac{\left(R_i + R_o\right)}{2} \tag{3}$$

This concept allows that, if changes in the geometry or discretization are made, the new spring stiffness can be determined from the constant *lps* without having to tune the former until the C-model results match those of the whole model.

Since the pipe should only be stiffened in the *x*-direction, the support of each spring on the extreme that is not attached to the pipe should only be restricted in that direction. This is a kinematic configuration (i.e. not entirely constrained), which cannot be handled in a linear static analysis. This is overcome by restraining the support in all directions, but placing it far away from the pipe so that the components on directions other than *x* are comparatively negligible.

C. Optimization

In the developed optimization procedure the shell models are created by utilizing B-splines (a detailed discussion can be found in Ref. 4). They describe the centerline, as well as the varying thickness of the cross section. To this end *k* key points *P* are generated, whose *x* and *y* coordinates, as well as thickness values are known.

The profile is then divided into three segments – two horizontal ones and one vertical one. Now the variation of the three values (coordinates and thickness) along a segment is described by means of the B-splines, which are governed by the control values b_i. The corresponding *x* and *y* component form a control point B_i. Four control points build a sub segment, which is bounded by two key points. A set of key points and the corresponding control points are depicted in Fig. 9. With the control values computed, the splines can be evaluated at arbitrary locations, yielding the interpolated value for a coordinate component or the thickness.

The advantage of the above procedure, in comparison to using the key points straight away without interpolation, becomes apparent when applied in optimization processes. Here the control points are the design variables and not the key nodes. Therefore the geometry model is optimized, rather than the FE model. This leads to a smaller number of design variables while no accuracy is sacrificed. Furthermore, nodes will not be moved in a way that a different discretization stiffens the system, rather than an improved geometry.

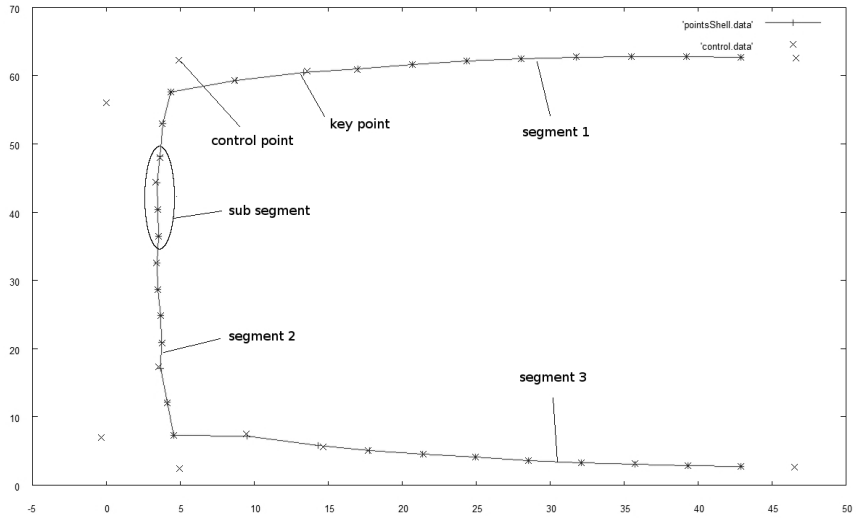

Figure 9: Key points and control points. Two key points and four control points build a sub segment. The cross section consists of three segments. Each segment is approximated by an individual B-spline.

Before the control values can be calculated the segments' end conditions have to be specified. There are two possible end conditions. The natural boundary condition, which features zero curvature at each end, is one. The advantage of that condition is that no tangent vectors have to be provided. One should be aware though, that this can cause kinks at intersections of segments. These kinks lead to the so called *C(0)* connectivity. *C(2)* connectivity, offering smooth transition from one segment to another, can be achieved by choosing the second end condition. Therefore tangent vectors have to be chosen in such a way, that they match at each intersection.

Once the control values are generated, a B-spline can be evaluated at an arbitrary position. This position is governed by the parameter *h*. This parameter starts with *0* at one key point and ends with *1* at the following.

With the B-spline definition completed, the optimization process can be constructed. The required elements are a program that can create the control points from discrete key points and thicknesses, as well as evaluate the B-splines to obtain discrete cross-sectional points and its corresponding thickness. Additionally, an FE program has to be available. In the present case this is FEAP (see Ref. 3), extended by a user developed mesh generation tool. The last part is a software that improves the design variables in order to obtain an optimal configuration of those. The sensititivities of the objective function and of the constraints, i.e. of the pipe stiffness and the stress constraints, required for this procedure, have to be calculated as well.

The developed optimization procedure is illustrated in Fig. 10 and can be described as follows: In a first step the control points of the B-splines are calculated and it is determined which are used as design variables. In case of size

optimization only those control values governing the thickness variation are used. In case of shape optimization also some of those describing the *x* and *y* coordinate variation are eligible.

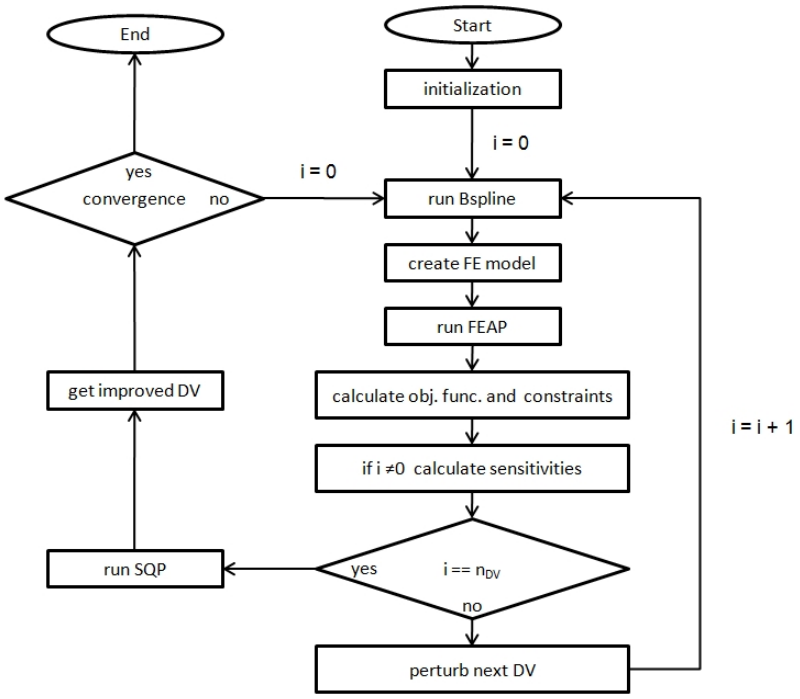

Figure 10: Flowchart of the optimization process. Three programs, B-spline, FEAP and an SQP optimizer, are coupled and can be used for size and shape optimization.

Now the optimization tool, in this case a Sequential Quadratic Programming (SQP) tool (the theoretical background can be found in Ref. 4), is initialized with the number of design variables and the number of constraints. Furthermore, the initial design variable values and their boundaries are defined. It returns the improved design variables.

Next, the FE analysis part starts. One analysis is conducted without changing any of the design variables. All the following results within the actual iteration will be related to that initial analysis. To run that initial analysis, the design variables from the SQP are read and via the B-spline tool the geometry is generated, which is converted into the FE model. After this simulation is accomplished, the resulting pipe stiffness, as well as the pipe's volume is stored.

Subsequently n_{DV} analyses are conducted, where n_{DV} is the number of design variables. These analyses differ by the design variable which is perturbed at the time. Comparing the resulting pipe stiffness and volume of the actual simulation with the initial one yields the corresponding sensitivity with respect to the active design variable. Naturally after an analysis with one perturbed design variable is finished, its pipe stiffness and volume are stored and its value is restored to the original one. This is repeated, until all design variables have been processed. The sensitivity of the objective function and the constraint with respect to the *i*-th design variable DV_i is computed according the finite difference method, shown in Eq. 4.

$$\frac{df}{dDV_i} = \frac{f(DV_i) - f(DV_i + \xi \cdot DV_i)}{\xi \cdot DV_i} \tag{4}$$

Here $f(DV_i)$ is either the objective function or a constraint of the initial configuration, whereas $f(DV_i + \xi \cdot DV_i)$ is the one of a configuration where the *i*-th design variable is perturbed by a small factor ξ. This perturbation factor was found to be best as 10^{-4}.

Now the values of the objective function and the constraint as well as the corresponding sensitivities are written to a file that is read by the SQP. It then returns a set of improved design variables. The whole procedure is repeated, until convergence occurs.

D. Application

The developed optimization procedure has been applied to two optimization tasks, a size and a shape optimization. In either case the employed model was the C-shell model with spring boundary of a 1500 mm diameter pipe. Both problems have been conducted with and without stress constraints in order to compare their results. The minimum and maximum thicknesses were set to 3 and 20 mm, respectively. In shape optimization the maximum allowed change of the *x* and *y* coordinates was set to 50 mm.

The first example is a thickness variation optimization of the cross-section with the objective to minimize the material per unit length of the pipe subject to a minimum stiffness requirement. Further constraints are that the absolute values of the stress tensor components, as well as minor and major principle stresses (all evaluated at the extremes of the element) do not increase with respect to the original profile. The optimization improves the pipe in two ways. A profile is obtained that is less conservative, that is to say it is closer to the requirements and a wall thickness variation that provides a higher stiffness than any other.

The second example is a shape optimization. The objective and constraints were identical to those in the preliminary example, only the number of design variables was increased. That means in the first case only the control values governing the thicknesses of the cross-section could be altered, whereas in the second case the design variables also included the control values describing the coordinates of the key points on the mid-surface of the profile.

III. Results

The resulting element thicknesses of the size optimization example without and with stress constraints are shown in Fig. 11 and the corresponding cross-sections in Fig. 12 and Fig. 13, respectively. The former corresponds to a material saving of around 46%, while the latter reached around 44%. Obviously the additional constraints do not have a significant impact on the material saving. Nevertheless it can be observed that, due to the stress constraints, the material is partly shifted from the middle of the horizontal walls to the upper corners. That indicates a stress concentration in those corners. The qualitative distribution though remains unchanged. Therefore only a slight change in the material saving occurs.

The resulting element thicknesses of the shape optimization example without and with stress constraints are shown in Fig. 14 and the corresponding cross-sections in Fig. 15 and Fig. 16, respectively. The former corresponds to a material saving of around 60%, while the latter reached around 47%. Thus the additional constraints have a significant impact on the material saving.

In the stress unconstrained case all thicknesses are reduced to its minimum. Since the objective is to reduce the area of the cross-section per unit length of the pipe, the profile width increases as much, as the boundaries allow, while the height is increased, until the required pipe stiffness is met. Thus the saved material is simply a function of the maximum allowed change of the coordinates. Naturally increasing the size of the profile infinitely also increases the stresses infinitely and therefore the optimization task does not yield realistic and serviceable results. For that reason further constraints that state maximum allowable stresses have to be added.

Their introduction forces the thicknesses in the upper corners and in the middle of the bottom wall to be increased. Though a wider profile leads to a higher material saving for the stress unconstrained shape optimization example this is not the case in the stress constrained case, because a wider profile leads to higher stresses which in return requires thicker walls. This would eliminate the positive effect and even reverse it. Thus the profile is widened only slightly. Of course less conservative stress constraints would lead to a larger profile and could magnify the difference in material saving capabilities between size and shape optimization.

The resulting profile obtained by shape optimization is thicker in the upper corners than the one from size optimization because of the higher stresses occurring in the slightly larger profile.

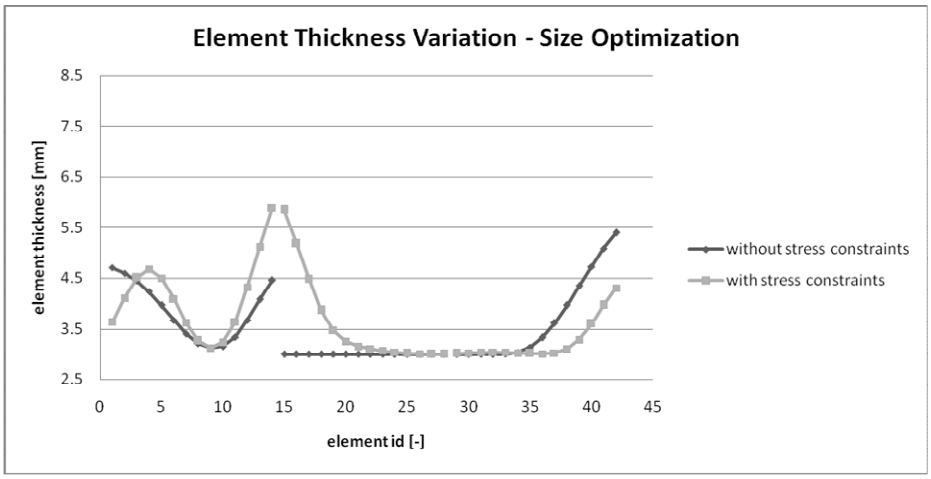

Figure 11: Wall thickness distributions as obtained by size optimization with and without stress constraints.

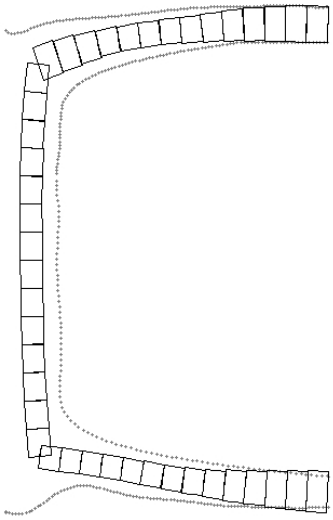

Figure 12: Original (dotted line) and optimized profile from size optimization without stress constraints.

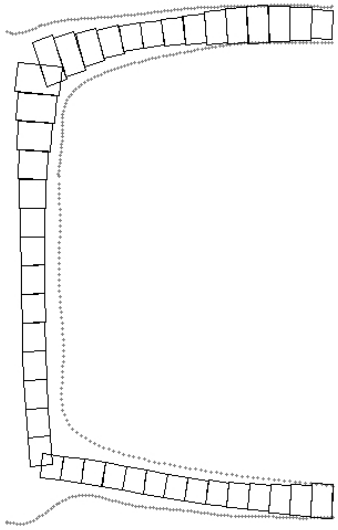

Figure 13: Original (dotted line) and optimized profile from size optimization with stress constraints.

In summary one can say that in size optimization the ringstiffness and the material saving are controlled by means of the thickness variation, while in shape optimization only the height is used for the ringstiffness adjustment while the width determines the material saving. The thicknesses are simply reduced until they reach their minimum value or until stress constraints become active.

Due to the fact that in shape optimization the only purpose of altering the thickness variation is to meet the stress constraints one can qualitatively observe to which degree a thickness in size optimization is increased due to stress constraints and to which due to the stiffness constraint. Comparing the thickness variation of the stress constrained size and shape optimization it becomes apparent that the middle of the upper horizontal wall contributes only towards the stiffness, whereas the middle of the bottom one contributes to some extend to both constraints. The latter is also the case for the upper corners.

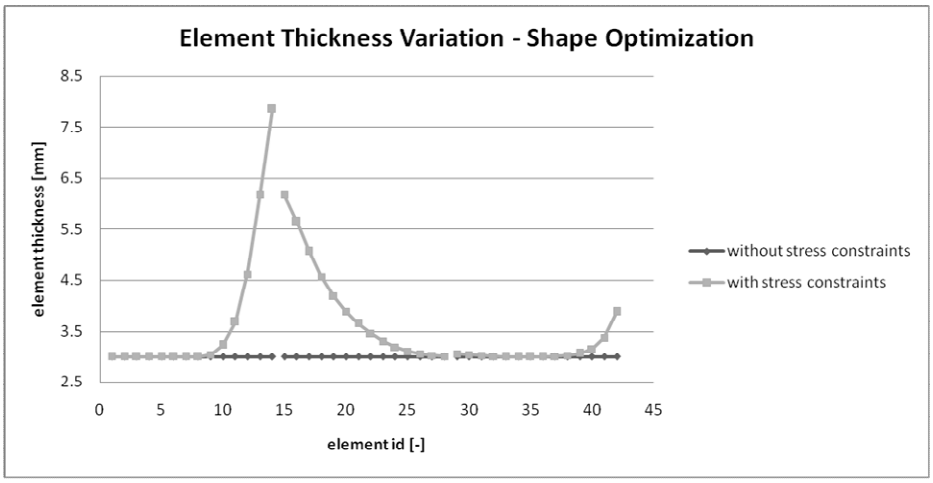

Figure 14: Wall thickness distributions as obtained by shape optimization with and without stress constraints.

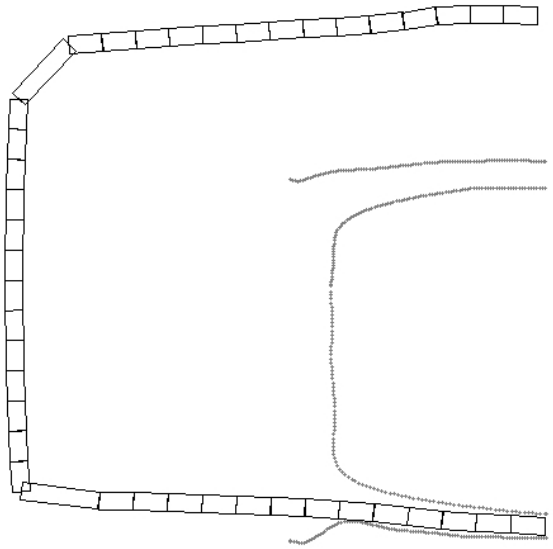

Figure 15: Original (dotted line) and optimized profile from shape optimization without stress constraints.

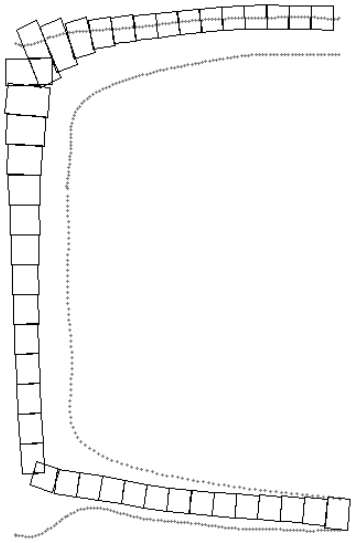

Figure 16: Original (dotted line) and optimized profile from shape optimization with stress constraints.

IV. Conclusions

FE models with different degrees of accuracy and efficiency where sought for simulating the pipe stiffness test according to the standard BS EN 1446: 1996. This was realized, and a Java Tool and several FORTRAN 77 programs were developed, that allowed for an automated generation of those models from scanned pipe profiles, which guaranteed realistic geometry data. With those models at hand, an optimization tool, based on the coupling of open-source and in-house software, was developed. It was applied to a size and a shape optimization task. Either one was conducted with and without stress constraints so that their influence could be investigated.

The size optimization example led to a material saving of 46% and 44% without and with stress constraints, respectively. The shape optimization example yielded 60% and 47%. The fact that the material saving in size optimization does not differ much whether stress constraints are omitted or not indicates how little influence it has

for this type of optimization. For shape optimization though the result is highly dependent upon them as the resulting profile changes to a larger extent. Therefore they have to be chosen carefully to take advantage of the material saving capabilities to full capacity. That is to say, rather than permitting the maximum stresses that occur in the original pipe less conservative values have to be found using material tests.

Furthermore, the optimization is restricted to design to best meet the requirements of the stiffness test. A good performance there does not mean a good pipe performance during installation and in service though. These load states differ significantly from the test and therefore have to be investigated in the future.

Acknowledgements

The first authors gratefully acknowledge the financial support from Asset International Ltd.

References

[1]British Standards Institution. "*Plastics piping and ducting systems – Thermoplastics pipes – Determination of ring flexibility*",*BS EN 1446 : 1996*, British Standards Institution, London, 1996.

[2]Berkeley University. "*FEAPpv Manual*", http://www.ce.berkeley.edu/~rlt/feappv, 2005.

[3]E. Hinton; J. Sienz; M. Özakça. "*Analysis and Optimization of Prismatic and Axisymmetric Shell Structure*", Springer-Verlag, London, 2003.